Biol. Cybern. 71, 417–431 (1994)

Biological Cybernetics

Generation of periodic and chaotic bursting in an excitable cell model

Yin-Shui Fan, Teresa Ree Chay

Department of Biological Sciences, Faculty of Arts and Sciences, University of Pittsburgh, Pittsburgh, PA 15260, USA

Received: 24 September 1993/Accepted in revised form: 16 April 1994

Abstract. There are interesting oscillatory phenomena associated with excitable cells that require theoretical insight. Some of these phenomena are: the threshold low amplitude oscillations before bursting in neuronal cells, the damped burst observed in muscle cells, the period-adding bifurcations without chaos in pancreatic β-cells, chaotic bursting and beating in neurons, and inverse period-doubling bifurcation in heart cells. The three variable model formulated by Chay provides a mathematical description of how excitable cells generate bursting action potentials. This model contains a slow dynamic variable which forms a basis for the underlying wave, a fast dynamic variable which causes spiking, and the membrane potential which is a dependent variable. In this paper, we use the Chay model to explain these oscillatory phenomena. The Poincaré return map approach is used to construct bifurcation diagrams with the 'slow' conductance (i.e., $g_{K,C}$) as the bifurcation parameter. These diagrams show that the system makes a transition from repetitive spiking to chaotic bursting as parameter $g_{K,C}$ is varied. Depending on the time kinetic constant of the fast variable (λ_n), however, the transition between burstings via period-adding bifurcation can occur even without chaos. Damped bursting is present in the Chay model over a certain range of $g_{K,C}$ and λ_n. In addition, a threshold sinusoidal oscillation was observed at certain values of $g_{K,C}$ before triggering action potentials. Probably this explains why the neuronal cells exhibit low-amplitude oscillations before bursting.

1 Introduction

Many excitable cells exhibit interesting types of electrical activity in response to external signals. For example, about 10% of guinea-pig inferior olivary neurons exhibit a low-amplitude threshold oscillation (Llinás and Yarom 1986). By a threshold oscillation, we mean a fast sinusoidal oscillation with a low amplitude. This oscillation is sinusoidal in shape and has a frequency of 4–6 Hz and an amplitude of 5–10 mV. Squid axons also generate a mixture of spikes and subthreshold oscillations when these cells are stimulated with a uniform depolarized current (Guttman and Barnhill 1970). Mouse pancreatic β-cells exhibit a period-adding sequence of bursting with increasing glucose concentration (Dean and Matthews, 1970). The β-cell bursting has a square wave appearance, and the spikes appear on the top of the plateau. When the glucose concentration reaches a suprathreshold concentration, the bursting transforms suddenly to continuous spiking without chaos. Canine colonic circular muscle exhibits a damped burst as well as a square wave burst in response to hormones and neurotransmitter (Huizinga et al. 1984a,b; Takeuchi 1978). In heart cells, an inverse period-doubling sequence has been observed in squid axons and molluscan neurons, in response to a train of current pulses (Guevara et al. 1981; Hayashi and Ishizuka 1987; Matsumoto et al. 1987).

In 1984, a three-variable model of an excitable cell was proposed as a mathematical description of periodic and chaotic behavior of excitable cells (Hindmarsh and Rose 1984), and a more physiologically refined three-variable model was elaborated by Chay (1985). The later model is a reduced form of the neuron cell models formulated by Plant (1981) and Chay (1983) and pancreatic β-cell models of Chay and Keizer (1983) and Lee et al. (1983). Since then, other bursting models have appeared in the literature, which contain three dynamic variables (Chay 1987; 1990a–c) and more than three dynamic variables (Canavier et al. 1991; Chay and Cook 1988; Chay and Fan 1993; Chay and Lee 1990; Epstein and Marder 1990; Rinzel and Lee 1987). The virtue of the original Chay model is its simplicity while generating all the essential features of electrical phenomena. The questions are: Does the three-variable model exhibit the interesting phenomena discussed above? If so, under what circumstances would it exhibit such phenomena? Does the system make the transition from periodic to aperiodic bursting endogenously? Although many investigators have studied bursting, spiking, and chaos using various types of excitable cell models, no one has attempted to answer the above questions using the bifurcation analysis approach employed in this paper.

Correspondence to: T. R. Chay

Chay (1985) and Kaas-Peterson (1987) examined the Chay model and computed periodic and chaotic bursting solutions for certain parameter values. Furthermore, the evidence obtained for the Rose–Hindmarsh model (Fan and Holden 1993; Holden and Fan 1992a–c), as well as for the Chay model (Fan and Chay 1993), shows that the transition from periodic to aperiodic bursting via very complicated dynamical behavior is a typical case of excitable membrane activity. How complex is it during the transition from periodicity to aperiodicity? Bifurcation analysis on the excitable cell models may give a clear understanding of these complex behaviors in excitable cell activity.

In this paper, we will explain how the Chay model gives rise to (1) a fast, low-amplitude, subthreshold oscillation observed by Guttman and Barnhill (1970) and Llinás and Yarom (1986); (2) a damped burst observed by Huizinga et al. (1984a, b) and Takeuchi (1978); and (3) periodic and chaotic burstings observed in the presence of epileptogenic and convulsant agents (Chalazonitis 1978). In Sect. 3, numerical investigations of (1) show that there are two thresholds. One occurs as the value, of the maximal conductance $g_{K,C}$ of the Ca^{2+}-sensitive K^+ channel passes through a threshold value at which the system abruptly triggers bursting action potentials. The other occurs over the parameter range of $\lambda_n \in [340, 380]$, where a phase change from multispike bursting to damped bursting gradually takes place. In Sect. 4, the Poincaré map approach to periodic and chaotic behavior was employed to present bifurcation diagrams with $g_{K,C}$ as the bifurcation parameter. The bifurcation diagrams represent the main dynamical features of the system and thus provide the best description of the system evolution as the parameter is varied. Period-doubling bifurcation gives rise to a transition from periodic to aperiodic bursting, and then inverse period-doubling bifurcation makes a transition from aperiodic back to periodic bursting. Additionally, some sudden transition from periodicity to aperiodicity and intermittent chaos induced by crisis (Fan and Chay 1993; Fan and Holden 1993; Grebogi et al. 1987; Holden and Fan 1992c) have also been observed in this model.

2 Model

The assumption of a 'mixed' effective conductance (Chay 1985) has been introduced to approximate the total inward current in terms of a single mixed conductance g_I, and reversal potential V_I. This mixed conductance represents the combination of the two functionally independent Na^+ and Ca^{2+} channels. This model is based on Hodgkin Huxley's excitable cell model (Hodgkin and Huxley 1952) and contains the following three simultaneous differential equations:

$$dV/dt = g_I m_\infty^3 h_\infty (V_I - V) + g_{K,V} n^4 (V_K - V) + g_{K,C} C/(1 + C)(V_K - V) + g_L (V_L - V)$$

$$dC/dt = \{m_\infty^3 h_\infty (V_C - V) - k_C C\}/\tau_C \quad (1)$$

$$dn/dt = (n_\infty - n)/\tau_n$$

where t is time, the independent variable. The dependent variables are V, the membrane potential; C, the dimensionless calcium concentration; and n, a probability of activation.

In (1), V_I, V_K, and V_L are the reversal potentials for 'mixed' $Na^+ - Ca^{2+}$, K^+, and leakage ions, respectively; g_I, $g_{K,V}$, $g_{K,C}$ and g_L are, respectively, the maximal conductances divided by the membrane capacitance; k_C is the rate constant for the efflux of intracellular Ca^{2+} ions; τ_C is a time constant which determines how fast C changes with respect to time; τ_n is the relaxation time of the voltage-gated K^+ channel, and n_∞ is the steady-state value of n. Note in (1) that the usual time dependencies of m and h in the Hodgkin-Huxley equations are replaced by their respective steady-state values.

Let y stand for h, m, or n, then the explicit expressions for h_∞, m_∞, and n_∞ can be written as

$$y_\infty = \alpha_y/(\alpha_y + \beta_y)$$

with

$$\alpha_h = 0.07 \exp(-0.05V - 2.5),$$

$$\beta_h = 1/(1 + \exp(-0.1V - 2)),$$

$$\alpha_m = 0.1(25 + V)/(1 - \exp(-0.1V - 2.5)),$$

$$\beta_m = 4 \exp(-(V + 50)/18), \quad (2)$$

$$\alpha_n = 0.01(20 + V)/(1 - \exp(-0.1V - 2)),$$

$$\beta_n = 0.125 \exp(-(V + 30)/80)$$

and

$$\tau_n = 1/(\lambda_n(\alpha_n + \beta_n))$$

$g_{K,C}$ and λ_n are the system control parameters. In this model, the parametric values are

$$g_I = 1800, g_{K,V} = 1700, g_L = 7;$$

$$V_I = 100, V_K = -75, V_L = -40, V_C = 100; \quad (3)$$

$$k_C = 3.3/18, \tau_C = 100/27$$

Some of the parametric constants in (2) and (3) differ from those in Chay (1985). Here we have made the parameters dimensionless constants.

In the model, C is a slow dynamic variable that causes the bursting, while n (gating kinetic variable of K^+ channels) is a voltage- and time-dependent fast dynamic variable that causes the spiking. The third dynamic variable is the membrane potential V, which is a dependent variable of both C and n.

3 Threshold phenomenon and phase transition of bursts action potentials

3.1 Notation

'Bursting' is a term used to describe the behavior of certain neurophysiological and chemical systems in

which periods of rapid spiking activity are separated by quiescent periods. Following the terminology used in Fan and Chay (1993); Fan and Holden (1993); Holden and Fan (1992a–c), the burst mode $\pi(j), j = 1, 2, \ldots$, stands for a bursting solution in which an orbit consists of j-spiking followed by a quiescent period. In this scheme mode $\pi(1)$ represents repetitive spiking; the burst mode $\pi(n, 2^m), n = 2, 3, \ldots, m = 1, 2, \ldots$ represents a bursting solution in which n-spikes alternate with a quiescent period 2^m times per orbit. For example, Fig. 1 (a1), (b1), (c), and (d) shows the burst modes $\pi(2)$, $\pi(2, 2)$, $\pi(3)$, and $\pi(3, 2)$, respectively, in the phase space; (a2) and (b2) are time series corresponding to (a1) and (b1), respectively.

3.2 The threshold value of $g_{K,C}$ that switches on the action potentials

Throughout this paper we use the parametric values given in (3), and we use λ_n and $g_{K,C}$ as the system control parameters. Numerical simulation for the model (1) shows that there is a threshold value $G^*_{K,C}$ at which the system switches on the action potentials. The threshold value $G^*_{K,C}$ differs slightly for different λ_n. This critical value is located in the interval $G^*_{K,C} \in (27.24, 27.26)$ for $\lambda_n \in [220, 500]$. For example, for $\lambda_n = 300$ the threshold value is located at $G^*_{K,C} \cong 27.245$, and for $\lambda_n = 350$ it is located at $G^*_{K,C} \cong 27.24$. As seen in Fig. 2, for $g_{K,C} > G^*_{K,C}$, the system exhibits either a stable steady state or a stable periodic oscillation with a very low amplitude. The stable steady state corresponds to the resting potential; the stable periodic oscillation corresponds to an attracting orbit in the phase space. The stable periodic oscillation is generated via a Hopf bifurcation. At the bifurcation, the stable steady state destabilizes as $g_{K,C}$ decreases. Since the Hopf bifurcation is a local mechanism, this type of oscillation oscillates with a very low amplitude and occurs in a very limited parameter range, $g_{K,C} \in (G^*_{K,C}, G^*_{K,C} + 0.02)$. For example, for $\lambda_n = 300$, the low-amplitude oscillation appears in the interval $g_{K,C} \in (27.245, 27.26)$. The low-amplitude oscillation fluctuates between -49 and -47. This kind of oscillation has been observed experimentally just prior to bursting (Guttman and Barnhill 1970; Llinás and Yarom 1986).

For $g_{K,C} \leqslant G^*_{K,C}$, the system switches on action potentials. Numerical experiments show that the bursting solution is suddenly triggered in the phase space as the parameter $g_{K,C}$ passes through the threshold value $G^*_{K,C}$. This kind of bursting solution possesses a high amplitude and fluctuates between -50 and -20. This periodic bursting is not directly generated from the previous, low-amplitude oscillation. It is activated after the low-amplitude oscillation destabilizes at the threshold value $G^*_{K,C}$.

The low-amplitude oscillation is a stable limit cycle. After the oscillation destabilizes, the orbit starting from any initial point no longer approaches the limit cycle. A new attractor is now formed in the phase space. The new attractor is a bursting solution. In Fig. 2, we show the occurrence of the system triggering bursting in terms of the representations of attractors in the phase plane V-C for two different parametric values.

Figure 2a shows how the system switches from a low-amplitude oscillation to a high-amplitude oscillation at $\lambda_n = 300$. Here, two periodic oscillations are plotted; the inner circle corresponds to the low-amplitude oscillation obtained before the threshold (i.e., $g_{K,C} = 27.247 > G^*_{K,C}$), and the outer orbit is the burst mode $\pi(6)$, with high amplitude, plotted after the threshold (i.e., $g_{K,C} = 27.245 \leqslant G^*_{K,C}$).

Figure 2b is obtained for $\lambda_n = 350$. This figure shows two oscillators, a low-amplitude one obtained at $g_{K,C} = 27.25$ and the burst mode $\pi(16)$ obtained at $g_{K,C} = 27.23$. These show that at the threshold value $G^*_{K,C}$ the system switches on action potentials. In addition, the system triggers action potentials with different burst modes for different values of $\lambda_n = [220, 310]$. In general, as λ_n increases, so does the number of spikes. This relation will be shown subsequently in Sect. 4 by constructing a bifurcation diagram for the model.

3.3 Phase transition between multi-spike bursting and damped bursting

As λ_n increases in the interval [340, 380], the Chay model undergoes a transition from multispike bursting to damped bursting. This behavior is shown in Fig. 3, where bursting solutions are projected in the phase plane V-C. Figure 3a–c, is obtained with λ_n at 340, 355, and 380, respectively, and with $g_{K,C} = 17$ in all cases.

Figure 3a1 shows a multispike burst mode $\pi(32)$ in the phase plane V-C, and a2 is the corresponding time series of the bursting solution. The multispike bursting mode consists of two parts: an initial decaying component and a later, diverging component. Figure 3b1 shows a burst mode appearing between a multispike burst mode and a damped burst mode, and b2, the corresponding time series. Figure 3c1 shows a damped bursting in the phase plane, and c2, the corresponding time series. During the damped bursting, spikings fluctuate as a damped oscillation and approach the transient plateau, and then drop to a quiescent period. Figure 3 shows that over the interval of $\lambda_n \in [340, 380]$ the system gradually transfers from a multi-spike burst mode to a damped burst mode, reflecting the gradual abolition of the diverging component.

For all values of $g_{K,C} \leqslant 27.24$, further numerical investigations reveal that the transition from multispike bursting to damped bursting occurs over the interval $\lambda_n \in [340, 380]$. For $\lambda_n \in (380, 500]$, the Chay model exhibits damped bursting. Such a damped bursting has been observed experimentally in some muscle cells (Huizinga et al. 1984a, b; Takeuchi; 1978). For $\lambda_n > 500$, the model gives simple oscillation (by simple oscillation, we mean a burst without spike on the top of the plateau). That is, as the maximum conductance $g_{K,C}$ increases, the Chay model makes a transition from multispike bursting to damped bursting and then to simple oscillation.

Multispike (square-wave) bursting and simple oscillation are quite different in many respects. The damped

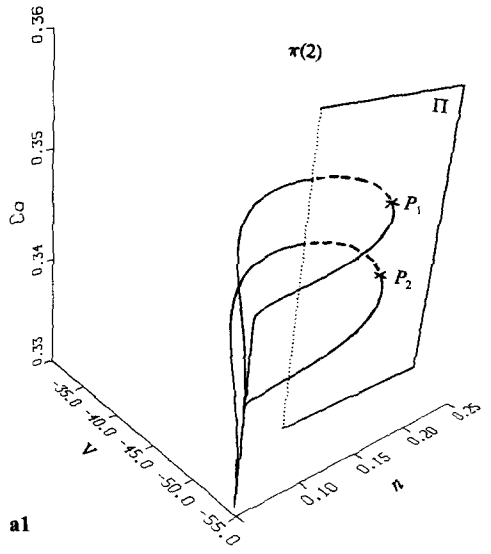

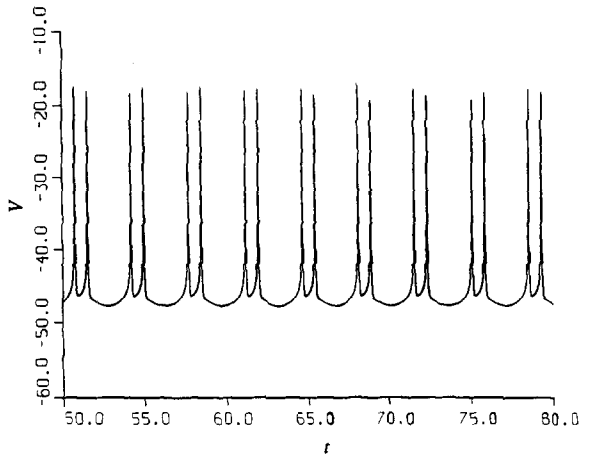

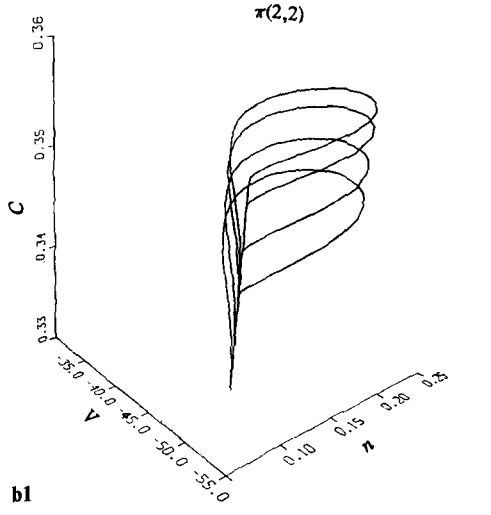

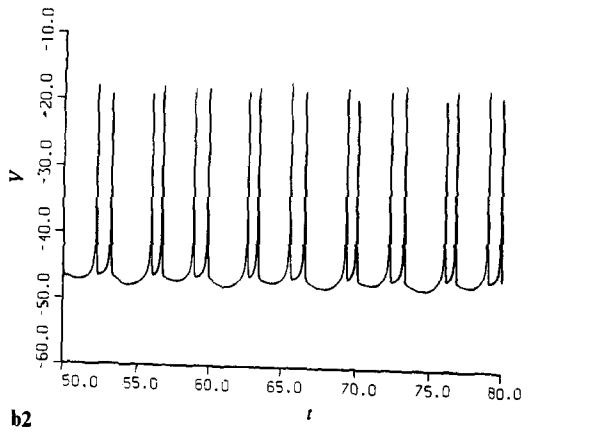

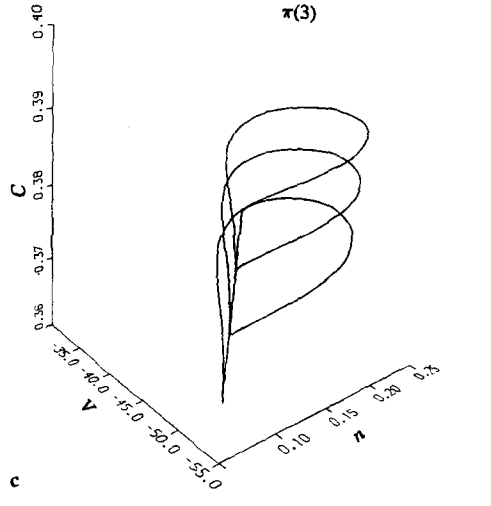

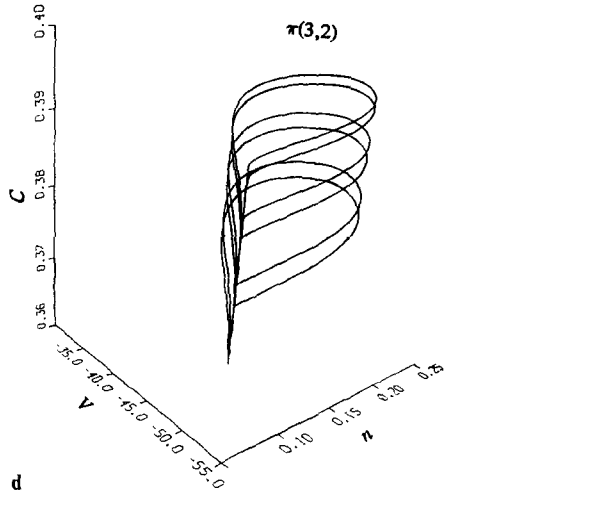

Fig. 1a–d. Phase space representations of burstings and the corresponding time series of (1). **a1** shows a burst mode $\pi(2)$ obtained for $\lambda_n = 220$ and $g_{K,C} = 13.75$, which intersects with the Poincaré section Π at two points, P_1 and P_2; **b1** burst mode $\pi(2,2)$, for $\lambda_n = 220$ and $g_{K,C} = 13.45$; **c** burst mode $\pi(3)$, for $\lambda_n = 225$ and $g_{K,C} = 12.7$; **d** burst mode $\pi(3,2)$, for $\lambda_n = 220$ and $g_{K,C} = 12.58$. **a2** and **b2** are time series of **a1** and **b1**, respectively

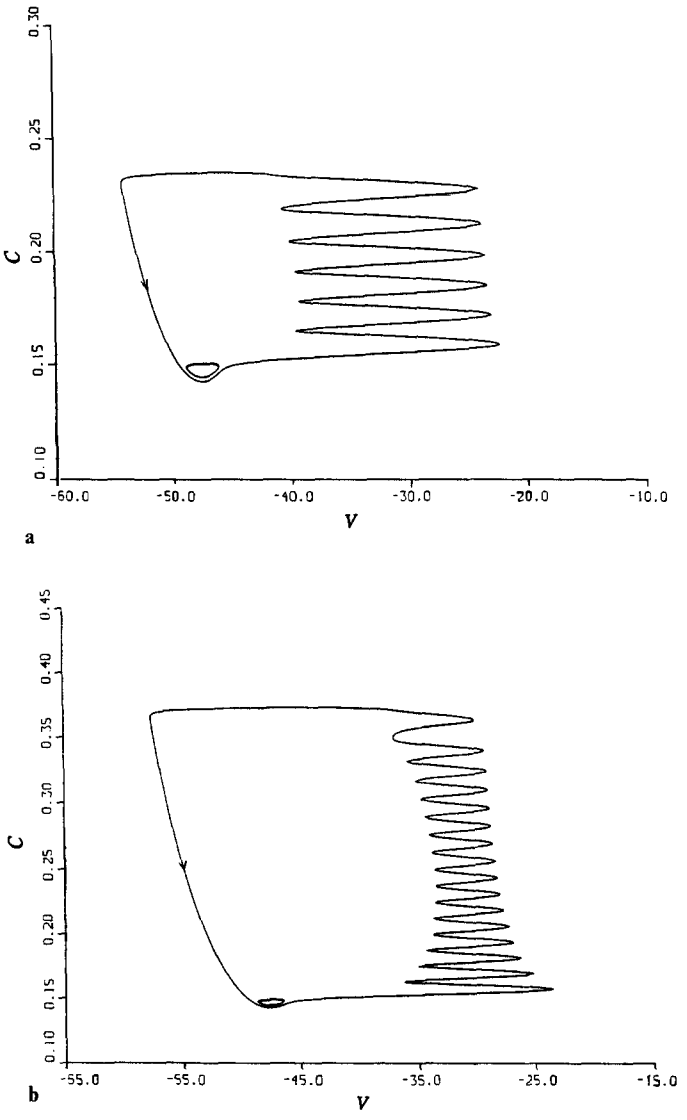

Fig. 2a, b. Representations of periodic oscillations and burstings in the phase plane V-C, showing that the Chay model triggers bursting action potential at threshold value $G^*_{K,C}$. **a** Obtained by numerical integration of (1) at $\lambda_n = 300$, and (i) the inner low-amplitude oscillation plotted for $g_{K,C} = 27.247 > G^*_{K,C}$, (ii) burst mode $\pi(6)$, the high-amplitude oscillation, for $g_{K,C} = 27.245 \leqslant G^*_{K,C}$; **b** obtained at $\lambda_n = 350$, and (i) the inner low-amplitude oscillation, for $g_{K,C} = 27.25 > G^*_{K,C}$, (ii) burst mode $\pi(16)$, the high-amplitude oscillation, for $g_{K,C} = 27.23 \leqslant G^*_{K,C}$

bursting occurs between multispike bursting and simple oscillation, and this bursting is different from the former two in many respects. All these three types of bursts have been seen experimentally (Dean and Matthews 1970; Huizinga et al. 1984a, b; Takeuchi 1978; Chay 1990c). It is interesting to note that the Chay model can reproduce all three types of bursts by simply varying the parameter $g_{K,C}$. We have shown how these three types of bursts transfer from one to another. Our bifurcation analysis clearly shows a phase transition from multispike bursting to damped bursting, and then to simple oscillation, as an accessible parameter varies.

4 The pattern of periodic and chaotic bursting generation

4.1 Poincaré map method

The Poincaré map approach to periodic and chaotic behaviors in nonlinear systems has been successfully used to reduce a highly dissipative system to a one-dimensional discrete system (Decroly and Goldbeter 1987; Fan and Chay 1993; Fan and Holden 1993; Holden and Fan 1992a–c; Poincaré 1899). The one-dimensional map was employed to detect periodic and chaotic regimes. In this section we shall construct the Poincaré maps for the model (1), which is defined by the intersection points of a trajectory with a Poincaré section in the phase space. We choose the plane

$$\Pi\colon V + 30 = 0 \tag{4}$$

as a Poincaré section of the Chay model, which is parallel to the phase plane C-n and transverses to the flows of the system. For example, Fig. 1a1 shows a 2-spike burst solution intersecting with the Poincaré section Π at the two points, $P_1(V_1, C_1, n_1)$ and $P_2(V_2, C_2, n_2)$. Defining a direct distance from point (V, C, n) in phase space to plane Π as follows

$$D = V + 30 \tag{5}$$

We say that a trajectory $O(t) = (V(t), C(t), n(t))$ of (1) intersects with plane Π at point (V^*, C^*, n^*) if (i) D vanishes at (V^*, C^*, n^*); (ii) $\mathrm{d}D/\mathrm{d}t|_{(V^*, C^*, n^*)} < 0$, where the complete derivative $\mathrm{d}D/\mathrm{d}t$ is taken along the trajectory $O(t)$. Condition (i) implies that the trajectory $O(t)$ intersects with Π at (V^*, C^*, n^*), and (ii) guarantees that only the intersections from one side of the Poincaré section are considered to form a Poincaré map. Thus, one can compute the intersections of the trajectory with the plane Π by numerically integrating (1).

Projecting the intersection points onto the phase plane n-C, these projection points form a nearly one-dimensional curve (denoted by Γ), shown in Fig. 4. This shows that the reduction of the model (1) to a one-dimensional map is reasonable for the Poincaré section Π. By numerically integrating (1), we construct the Poincaré map in the following way. Let $O(t, V_0, C_0, n_0)$ be a trajectory starting from the initial point $(V_0, C_0, n_0) \in \Gamma$. For successive intersections of the trajectory with the Poincaré plane Π, we denote these points by (V_N, C_N, n_N), $N = 0, 1, 2, \ldots$. Hence we obtain a discrete series $\{C_N\}_0^\infty$ of C values. Defining the $(N+1)$th value C_{N+1} as a function of the Nth, we therefore have a map

$$f\colon C_N \to C_{N+1},\ N = 0, 1, 2, \ldots$$

defined on the one-dimensional curve Γ. Each point on the one-dimensional curve Γ means that the orbit $O(t, V_0, C_0, n_0)$ of (1) intersects the Poincaré section Π at it. For example, in the case depicted in Fig . 1a1, there will be two different points, P_1 and P_2, situated in the one-dimensional curve Γ. These two points are the intersection points of the two spikes of burst mode $\pi(2)$ with Poincaré section (4). Therefore, the Poincaré maps constructed as above allow us to count the number of intersection points of an orbit with the Poincaré section. For

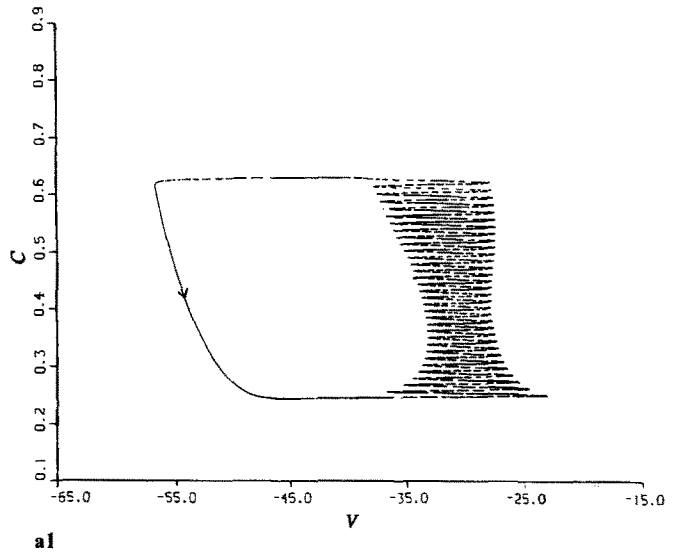

a1

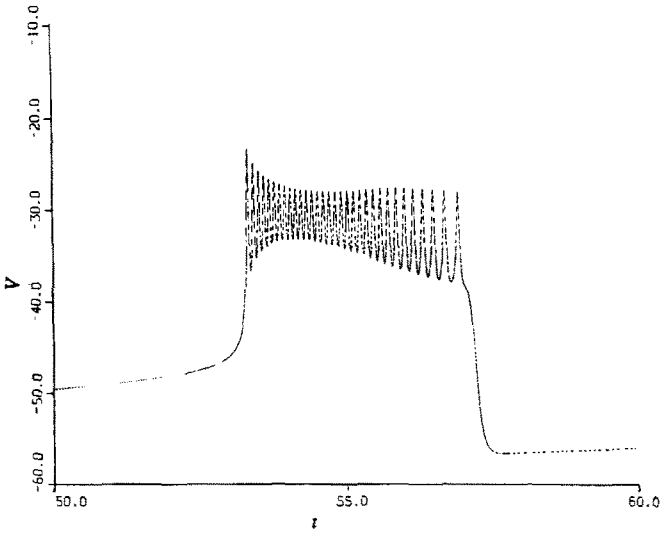

a2

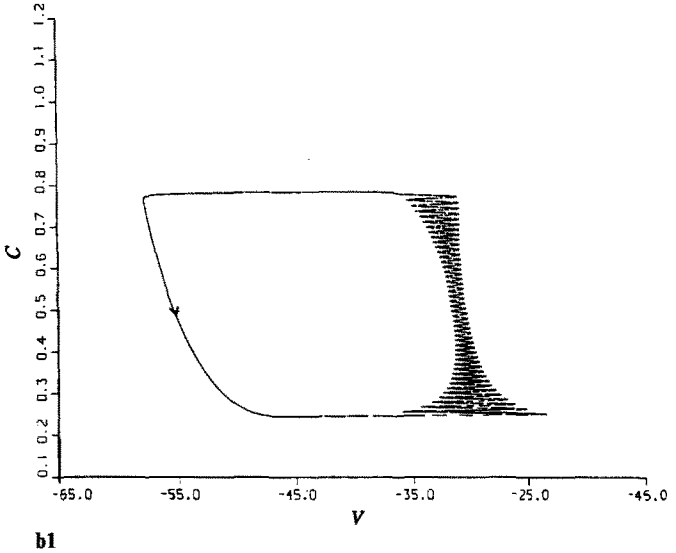

b1

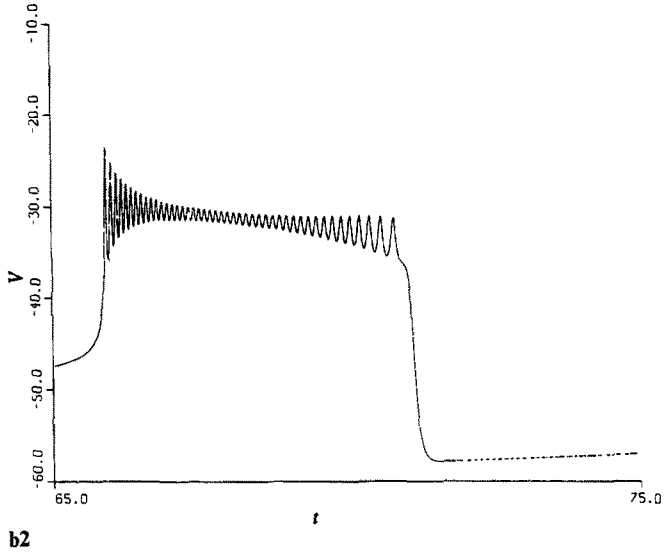

b2

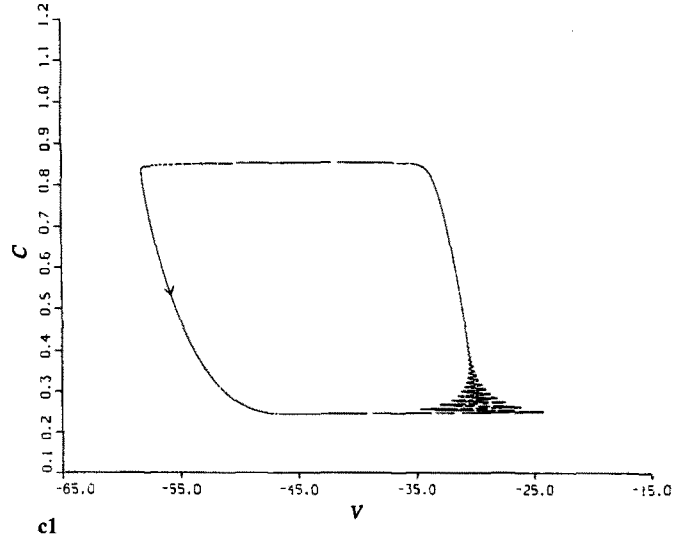

c1

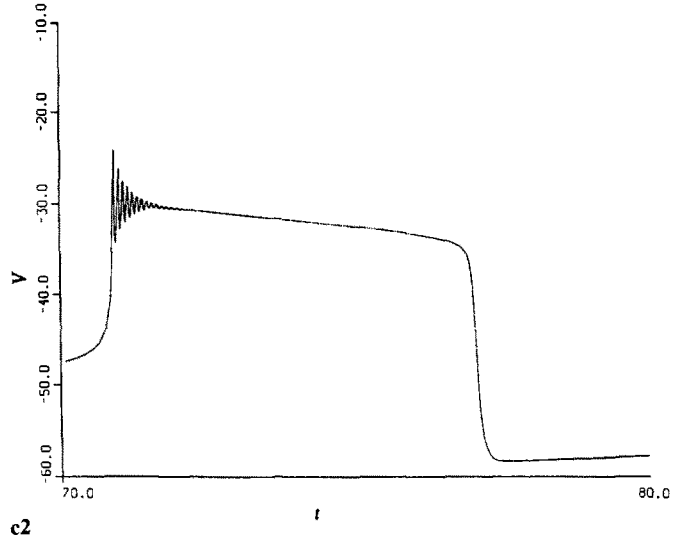

c2

Fig. 3a–c. Showing the phase change from multispike bursting to damped bursting over the interval of $\lambda_n \in [340, 380]$. **a1**, **b1** and **c1** are representations of burstings in the phase plane *V*-*C*, plotted with the same value of $g_{K,C} = 17$: **a1** the burst mode $\pi(32)$, for $\lambda_n = 340$; **b1** $\lambda_n = 355$; **c1** a damped bursting, for $\lambda_n = 380$. **a2**, **b2** and **c2** are the corresponding time series of **a1**, **b1** and **c1**, respectively

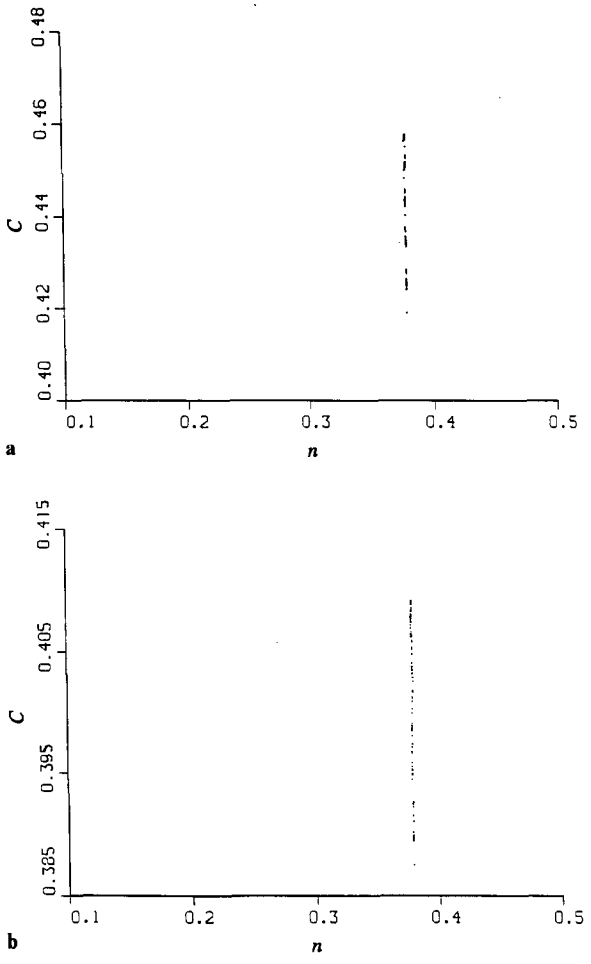

Fig. 4a, b. Intersection of an attractor with the Poincaré section Π is shown projected to the phase plane n-C, which forms a nearly one-dimensional curve Γ: **a** $\lambda_n = 230$ and $g_{K,C} = 11.3$; **b** $\lambda_n = 225$ and $g_{K,C} = 12.1$

each parameter value of $g_{K,C}$, an associated Poincaré map can be constructed, and the number of the intersection points with the Poincaré section can be counted; that is, the corresponding burst mode can be known in this way.

Figure 5 represents several Poincaré maps plotted by numerical integrations of (1) for different parameters. The map shown in Fig. 5b is associated with a periodic regime, a burst mode $\pi(27)$. The maps shown in Fig. 5a, c, and d are associated with chaotic regimes.

We note here that there are several choices for a Poincaré section, and the above special choice of Poincaré section (4) does not change the main qualitative dynamical features of the nonlinear system (Fan and Chay 1993; Holden and Fan 1992a–c). For example, if one chooses the plane $n - 0.25 = 0$ as a Poincaré section, the Poincaré maps constructed from this will be completely similar to those constructed from (4). If the plane C = constant is used as a Poincaré section, one will construct a two-dimensional Poincaré map from this. The two-dimensional Poincaré maps of the nonlinear system still reflect the intrinsic dynamical behaviors such as various bifurcations and chaotic activity.

4.2 Bifurcation diagrams

Having constructed the associated Poincaré map for (1), one can readily present bifurcation diagrams with $g_{K,C}$ as the bifurcation parameter. Figure 6 presents bifurcation diagrams over the parameter range of $g_{K,C}$ for $\lambda_n =$ 220, 225, 230, 300, and 500. In these diagrams, for each value of the bifurcation parameter ($g_{K,C}$ or λ_n) the points represent the dynamical behavior of the calcium concentration C. Since each point (corresponding to a value of C) in the diagrams is extracted from a phase point $(V, C, n) \in \Gamma$ and each point in the diagrams corresponds to a spike of a burst solution, the points in the diagram also reflect the behavior of membrane potential V. That is, each point in these diagrams also stands for a spike in membrane potential V. For example, in the case shown in Fig. 1a1, there are two points, C_1 and C_2, plotted in the bifurcation diagram. These two points in a bifurcation diagram represent a 2-spike bursting oscillation in the calcium concentration C, as well as exhibiting two spikes in the membrane potential V, as seen in Fig. 1a2.

From Figure 6a–c, for $\lambda_n \in [220, 230]$ the system evolves from simple bursting to repetitive spiking via chaos. This behavior is similar to that observed in the Rose–Hindmarsh model (Hindmarsh and Rose 1982, 1984). During this transition, the period-doubling bifurcation sequence cascades to chaos, and then inverse period-doubling bifurcation (Holden and Fan 1992a) gives rise back to repetitive spiking. The period-doubling and inverse period-doubling scenario can be observed in Fig. 6a1 and b1 or in Fig. 6a2 and b2. Inverse bifurcating phenomena have also been observed in the Rose–Hindmarsh model for neuronal activity (Holden and Fan 1992b), as well as in periodically stimulated cardiac cells (Guevara et al. 1981). The inverse bifurcation scenario gives rise to the transition from chaos to a periodic regime in these realistic systems.

Notice from Fig. 6b1 that at $g_{K,C} = 14.01$, the system suddenly ends the chaotic regime and exhibits a periodic burst mode $\pi(3)$. This kind of transition was viewed as saddle-node bifurcation (Guckenheimer and Holmes 1983; Hao 1983). At the saddle-node bifurcation, the system generates a periodic orbit of the saddle-node form and terminates chaos simultaneously. The saddle-node bifurcation was observed in many dissipative systems (Fan and Chay 1993; Guckenheimer and Holmes 1983; Hao 1983; Holden and Fan 1992a–c; May 1976) and is believed to be a self-reorganization mechanism. After the bifurcation, the system exhibits a (stable) period-3 orbit of the node form and a (unstable) period-3 orbit of the saddle form. In Fig. 6b1 and b2, only the stable period-3 orbit could be plotted after the saddle-node bifurcation at $g_{K,C} = 14.01$. One can also see an inverse saddle-node bifurcation at $g_{K,C} = 11.55$ in Fig. 6b2. Consequently, as $g_{K,C}$ is decreased, the evolution of the system from simple to repetitive spiking via the chaotic regime can be summarized by burst modes and chaotic regimes which present in the process as follows:

$$\pi(1) \rightarrow$$

$$\pi(2) \rightarrow \pi(2,2) \rightarrow \pi(2,2^2) \rightarrow \cdots \rightarrow \text{chaos} \rightarrow$$

$$\pi(3) \rightarrow \pi(3,2) \rightarrow \pi(3,2^2) \rightarrow \cdots \rightarrow \text{chaos}$$

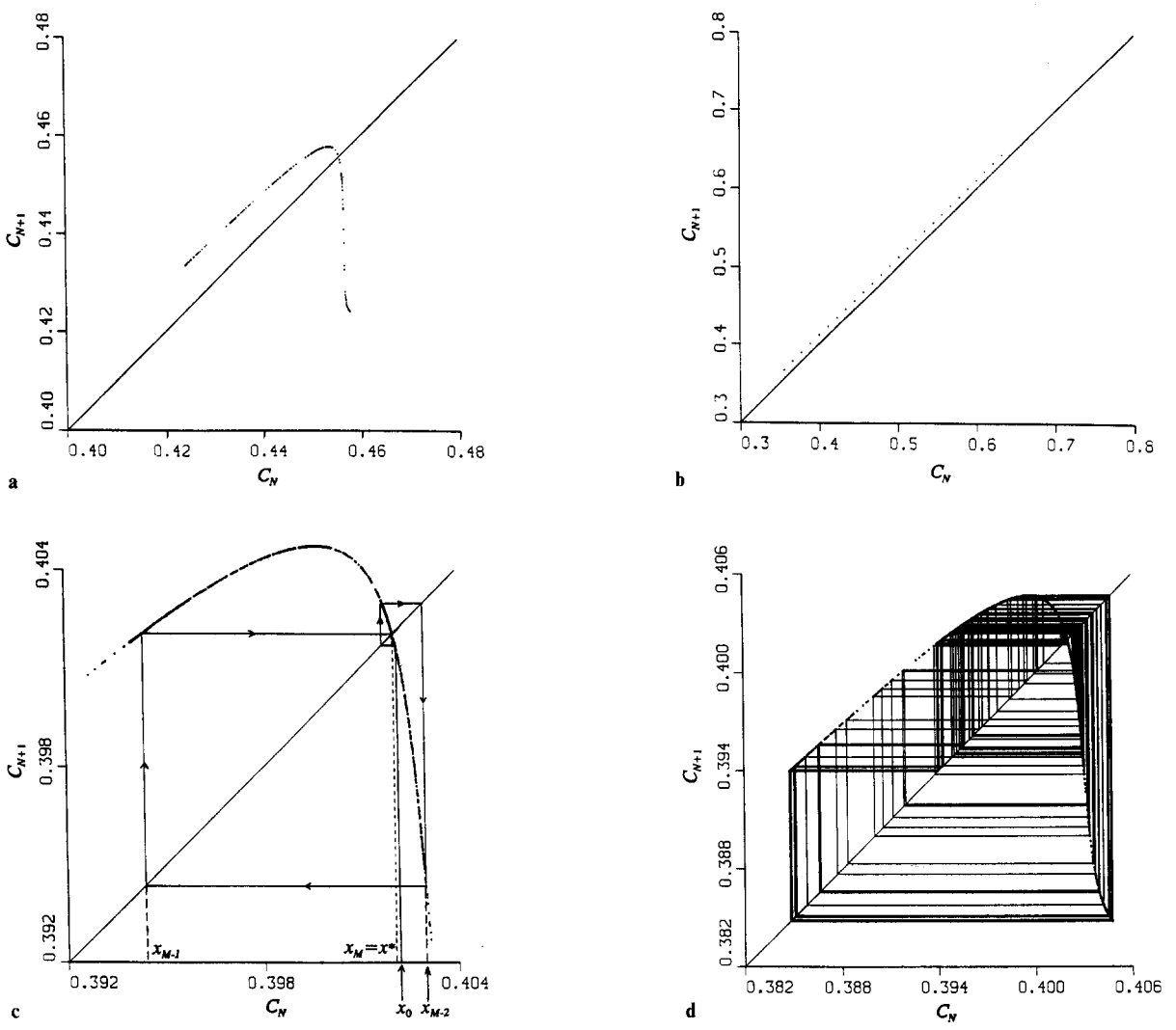

Fig. 5a–d. Poincaré maps obtained by numerically integrating (1): **a** $\lambda_n = 230$, $g_{K,C} = 11.31$; **b** $\lambda_n = 300$, $g_{K,C} = 12.92$; **c** $\lambda_n = 225$, $g_{K,C} = 12.2$, showing an orbit, $x_0, x_1, \ldots, x_{M-1}, x_M = x^*$, starting at an initial point x_0 (close to x^*); **d** a chaotic orbit in the presence of a snap-back repeller, with the same parameter as **c**

Central chaos

chaos $\rightarrow \cdots \rightarrow \pi(3, 2^2) \rightarrow \pi(3, 2) \rightarrow \pi(3) \rightarrow$

chaos $\rightarrow \cdots \rightarrow \pi(2, 2^2) \rightarrow \pi(2, 2) \rightarrow \pi(2) \rightarrow$

$\pi(1) \rightarrow$

In the sequence, every two successive burst modes are associated with a corresponding bifurcation, period-doubling or saddle-node. The period-doubling bifurcation sequence cascades to chaos, and saddle-node bifurcation undergoes a transition between periodicity and aperiodicity. The central chaotic range bridges two opposite bifurcation scenarios, the bifurcation and the inverse bifurcation process. After central chaos, the inverse bifurcation scenario gives rise to the transition from chaos back to periodic behavior. For $\lambda_n = 220$, the central chaotic range is over the interval $g_{K,C} \in (12.48, 13.2)$, see Fig. 6a2. For $\lambda_n = 225$, there are three chaotic ranges, and the central one is located in the interval $g_{K,C} \in (11.64, 12.57)$, see Fig. 6b2.

Period-doubling bifurcation cascade is a typical route from periodicity into chaos. This route has been described both in some one-dimensional maps (Guckenheimer and Holmes 1983; Hao 1983; May 1976) and in some continuous dissipative systems (Decroly and Goldbeter 1987; Holden and Fan 1992a, b). We showed in Fig. 1 the occurrence of period-doubling bifurcation in terms of the phase space representation of burst. Figure 1a1 and b1 shows a doubling process from the burst mode $\pi(2)$ to the mode $\pi(2, 2)$, and Fig. 1c and d, a doubling process from the burst mode $\pi(3)$ to the mode $\pi(3, 2)$.

Fig. 6a–e. Bifurcation diagrams obtained by numerically integrating (1). In **a1**, **b1**, **c1**, **d**, and **e**, we plot the dynamical behavior of the calcium concentration C as a function of $g_{K,C}$ for 5 different values of λ_n: **a1** $\lambda_n = 220$, **b1** $\lambda_n = 225$; **c1** $\lambda_n = 230$; **d** $\lambda_n = 300$; and **e** $\lambda_n = 500$. In addition, **a2** is the enlarged part of **a1** over the interval of $g_{K,C} \in [12.2, 13.7]$; **b2** the enlarged part of **b1** over the interval of $g_{K,C} \in [11, 12.7]$; **c2** the enlarged part of **c1** over the interval of $g_{K,C} \in [10.5, 12.5]$

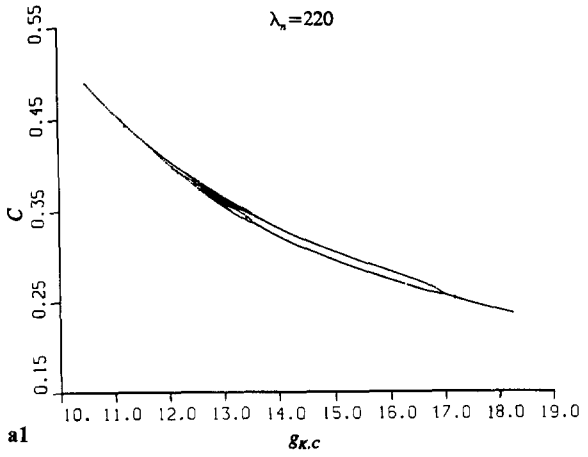

a1

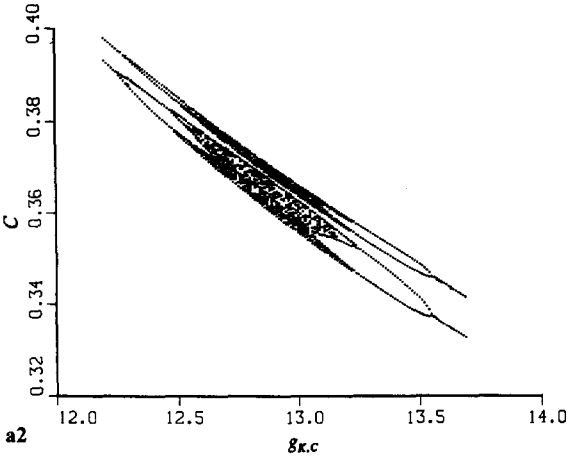

a2

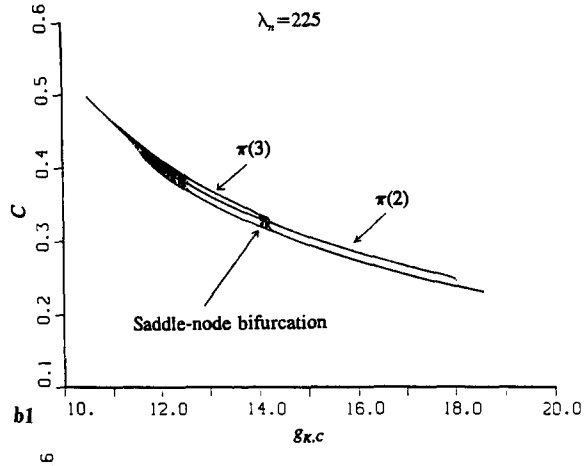

b1

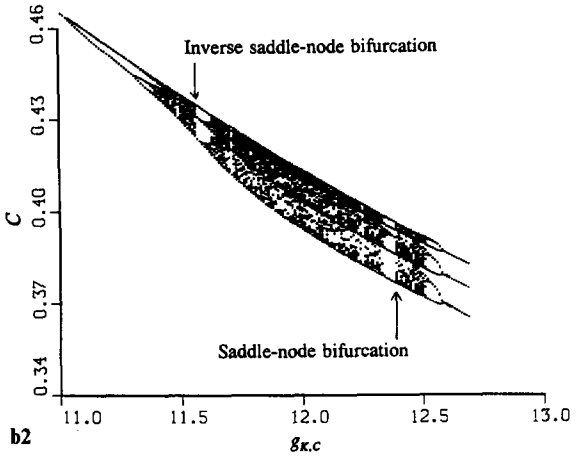

b2

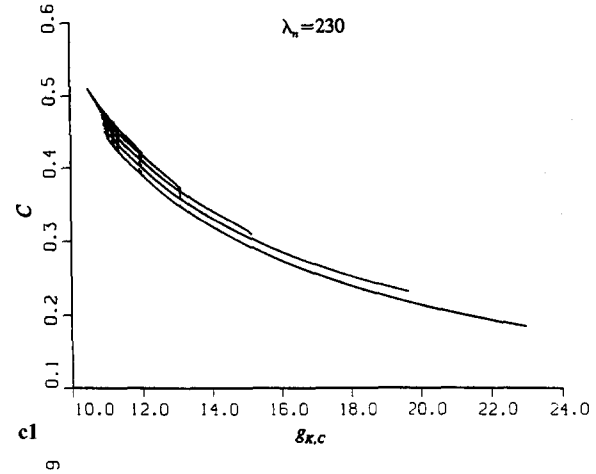

c1

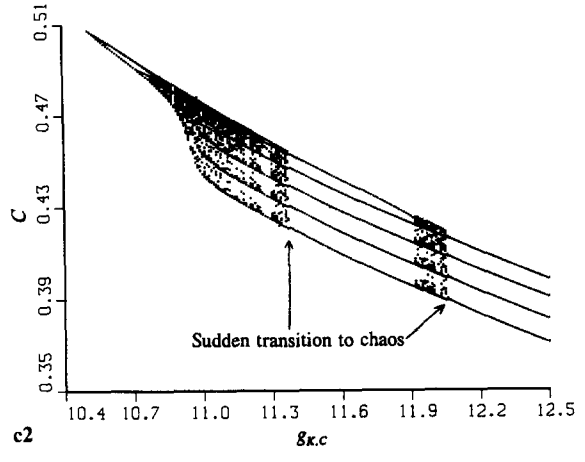

c2

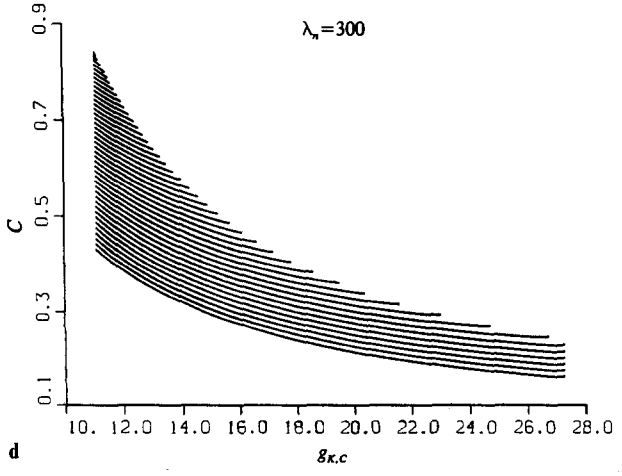

d

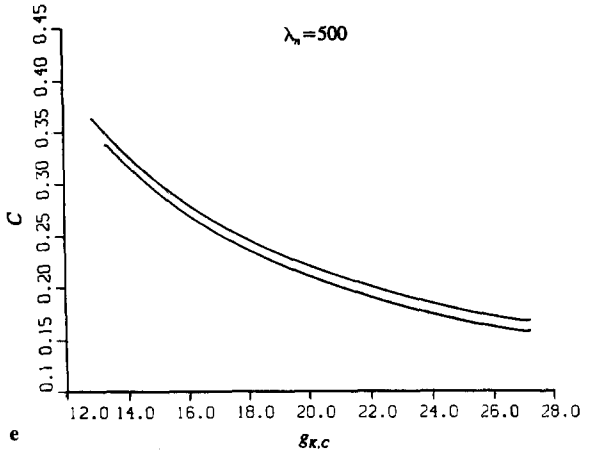

e

Whenever this kind of bifurcation occurs, the number of spikes in a burst will be doubled. For example, the burst mode $\pi(3)$ bifurcates into $\pi(3,2)$ as if the previous burst $\pi(3)$ is split into a twin burst. This implies that the period of a burst is also doubled (Canavier et al. 1990; Chay 1984) as this bifurcation occurs. Generally, the period of burst mode $\pi(n, 2^m)$ is approximately equal to twice the period of burst mode $\pi(n, 2^{m-1})$.

Figure 6c1 is obtained for $\lambda_n = 230$. It also shows a transition from simple to repetitive spiking via chaotic regimes. As the parameter $g_{K,C}$ decreases, however, there is no apparent period-doubling bifurcation on the right side of Fig. 6c1. The bifurcation structure on the right part of the diagram in Fig. 6c1 is not the same as that in Fig. 6a1 and b1. Over this range, there are some intermittent chaotic regimes between the period-adding bifurcations. This chaos is not via period-doubling bifurcation cascades but via a sudden transition, as seen in Fig. 6c2. This kind of chaos has been viewed as crisis-induced chaos (Fan and Chay 1993; Fan and Holden 1993; Holden and Fan 1992c). For $\lambda_n = 230$, we find that this kind of chaos occurs in the range of $g_{K,C} \in [13.1, 13.13]$, [11.93, 12.05] and [10.82, 11.36], where the periodic behavior abruptly becomes intermittently aperiodic. As the parameter decreases further, the inverse period-doubling bifurcation sequence can be observed on the left part of the diagram in Fig. 6c1 and c2. Here chaos transforms to repetitive spiking via inverse period-doubling bifurcation.

Figure 6d plotted for $\lambda_n = 300$ shows a completely new picture. The entire evolution of the system over the interval $g_{K,C} \in [11, 27.24]$ is dominated by period-adding bifurcation (Fan and Holden 1993; Holden and Fan 1992a–c), and the system generates periodic bursting by this bifurcation. There is no chaos for $\lambda_n = 300$. Period-adding bifurcation has also been described by the Rose–Hindmarsh model of neurones. This period-adding bifurcation makes a transition between two different periodic regimes. At the threshold value $G^*_{K,C} = 27.245$, the system switches on action potentials with a burst mode $\pi(6)$. From then on, the number of spikes of the periodic burst of the system is increased by adding one spike to the previous burst every time the bifurcation occurs. This kind of bifurcation gives rise to the existence of multispike bursting. For example, for $\lambda_n = 300$ and $g_{K,C} = 11$, the system exhibits 44-spike bursts as shown in Fig. 7. As $g_{K,C}$ decreases further, we find that the Chay model undergoes a crisis at $g_{K,C} \simeq 9.675$, as described in Fan and Chay (1993). At the crisis, the system makes a transition from multispike bursting to chaotic spiking for certain parametric values. After the crisis, inverse bifurcation leads from chaos to repetitive spiking.

Figure 6e is plotted for $\lambda_n = 500$. At this parametric value, the Chay model exhibits damped bursting oscillation. The reason the diagram depicts burst mode $\pi(2)$ is that the only two high-amplitude spikes of these damped burstings intersect with the Poincaré section Π, while the low-amplitude spikes missed intersecting with the Poincaré section.

The diagram in Fig. 8 has λ_n as the bifurcation parameter, for a fixed value of $g_{K,C} = 27.24$. It shows that for

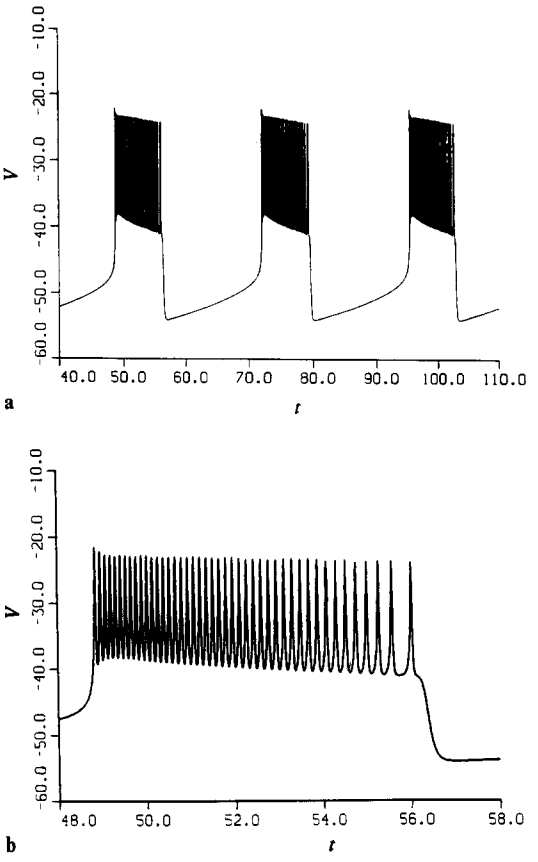

Fig. 7. **a** Time series of burst mode $\pi(44)$, plotted for $\lambda_n = 300$ and $g_{K,C} = 11$; **b** an enlarged part of **a**

different values of $\lambda_n \in [220, 310]$ the Chay model produces different burst modes at the threshold value $G^*_{K,C} = 27.24$. As λ_n increases, so does the number of spikes.

Figure 9, plotted for $\lambda_n = 225$ and $g_{K,C} = 12.1$, shows chaotic bursting in terms of phase space representation and time series, respectively. In the case of chaotic bursting, the behavior of the trajectory is unpredictable, and the kinetics of both calcium concentration C and membrane potential V exhibit random behavior.

4.3 The pattern of periodic and chaotic bursting

By analysing our results from which the bifurcation diagrams were plotted, we can present the pattern of burst modes over the region of parameter $g_{K,C}$. The generation of periodic and chaotic bursting can be represented in more detail in the burst regime. In Table 1, the first column lists the behavioral modes that exist in the Chay model. The second and third columns list the intervals of $g_{K,C}$ for which the burst modes in the first column exist. These two columns were obtained at $\lambda_n = 220$ and $\lambda_n = 225$, respectively.

Table 2 gives the bifurcation values and the burst modes depicted by Fig. 6d, for $\lambda_n = 300$. The first column is the behavioral modes present in Fig. 6d; the second column lists the intervals of $g_{K,C}$ in

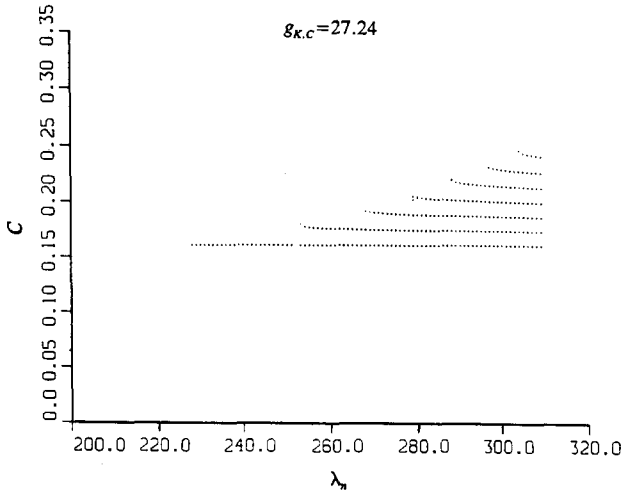

Fig. 8. Plotted for $g_{K,C}=27.24$, with λ_n as a bifurcation parameter, different kinds of burst mode are triggered at threshold value $G^*_{K,C}$ for different $\lambda_n \in [220, 310]$

which the corresponding burst modes in the first column occur.

Table 3, corresponding to Fig. 8, shows that for different values of $\lambda_n \in [220, 310]$ the Chay model exhibits different burst modes at the threshold value $G^*_{K,C} = 27.24$. As λ_n increases, the number of spikes increases.

4.4 A qualitative diagnosis for chaos

In the previous sections, we have examined and observed chaos from bifurcation diagrams for model (1). We shall demonstrate qualitatively that some Poincaré maps obtained by numerically integrating (1) exhibit deterministic chaos. As an example, we consider the Poincaré map f plotted in Fig. 5c for $\lambda_n = 225$ and $g_{K,C} = 12.2$. Numerical analysis shows that $x^* = 0.402071$ is a fixed point of f. We say the fixed point x^* is a snap-back repeller (Marotto 1978), if (1) $|f'(x^*)| > 1$; (2) for any real $r > 0$ and a neighborhood $N_r(x^*)$ of x^*, there exists a point $x_0 \in N_r(x^*)$ and $x_0 \neq x^*$ such that $f^M(x_0) = x^*$, $\mathrm{d}f^M(x_0) \neq 0$ for some positive integer M.

We now prove that the Poincaré map shown in Fig. 5c is chaotic by examining the existence of a snap-back repeller for the map f. Consider the following sequence obtained by iterating the map f:

$$x_0 = f_R^{-M}(x^*), \ldots, x_{M-2} = f_R^{-2}(x^*), x_{M-1} = f_R^{-1}(x^*), x^*$$

Here $f_R^{-N}(x)$, $N = 1, 2, \ldots, M$, denotes the Nth pre-image of x in the sense that we take the right one if two pre-images exist. The sequence is an orbit of the Poincaré map f and is given as the solid line with arrows in Fig. 5c. It meets:

(i) $\mathrm{d}f(x_i)/\mathrm{d}x \neq 0, i = 1, 2, \ldots, M$, and $\mathrm{d}f^M(x_0)/\mathrm{d}x \neq 0$
(ii) for any real $r > 0$ and $N_r(x^*)$, there must be an integer $M > 0$ such that $x_0 \in N_r(x^*)$
(iii) $f^M(x_0) = x^*$
(iv) $|\mathrm{d}f(x^*)/\mathrm{d}x| = 3.42 > 1$ (obtained numerically)

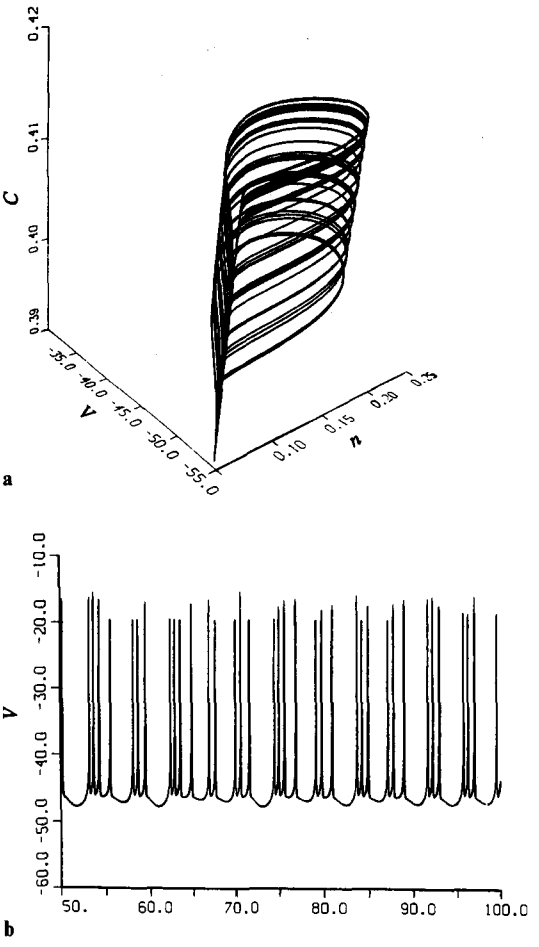

Fig. 9a. Chaotic attractor plotted by numerical integration of (1) for $\lambda_n = 225$ and $g_{K,C} = 12.1$; **b** the time series corresponding to **a**

Table 1. Range of the occurrence of the different behavioural modes, as a function of $g_{K,C}$, for $\lambda_n = 220$ and 225

Behavioral modes	Intervals of $g_{K,C}$ at $\lambda_n = 220$	Intervals of $g_{K,C}$ at $\lambda_n = 225$
$\pi(1)$	[17.01, 27.24][b]	[18.06, 27.24]
$\pi(2)$	[13.68, 16.98]	[14.28, 18.03]
$\pi(2, 2)$	[13.23, 13.65]	14.25
...	...	...
PD[a] & chaos	[12.48, 13.20]	[14.04, 14,2]
$\pi(3)$		[12.66, 14.01]
$\pi(3, 2)$		[12.60, 12.63]
...		...
PD & central chaos		[11.64, 12.57]
...		...
$\pi(3, 2)$		11.61
$\pi(3)$		11.58
PD & chaos	[12.48, 13.20]	[11.40, 11.55]
...	...	...
$\pi(2, 2)$	[12.33, 12.45][b]	[11.34, 11.37]
$\pi(2)$	[11.76, 12.30]	[11.04, 11.31]
$\pi(1)$	[10.00, 11.73]	[10.00, 11.01]

[a] Stands for period-doubling bifurcation sequence
[b] The left-end point of interval embedded in bifurcation range and the right-end point of the interval in inverse bifurcation range is an approximate bifurcation value, at which an associated bifurcation occurs

Table 2. Range of occurrence of the different behavioural modes, as a function of $g_{K,C}$, for $\lambda_n = 300$

Burst modes	Intervals of $g_{K,C}$ at $\lambda_n = 300$
$\pi(6)$	[26.70, 27.24]
$\pi(7)$	[24.72, 26.67]
$\pi(8)$	[24.69, 23.01]
$\pi(9)$	[21.60, 22.98]
$\pi(10)$	[20.40, 21.57]
$\pi(11)$	[19.41, 20.37]
$\pi(12)$	[18.57, 19.38]
$\pi(13)$	[17.82, 18.54]
$\pi(14)$	[17.19, 17.79]
$\pi(15)$	[16.62, 17.16]
$\pi(16)$	[16.11, 16.59]
$\pi(17)$	[15.69, 16.08]
$\pi(18)$	[15.27, 15.66]
$\pi(19)$	[14.91, 15.24]
$\pi(20)$	[14.50, 14.88]
$\pi(21)$	[14.28, 14.55]
$\pi(22)$	[14.01, 14.25]
$\pi(23)$	[13.74, 13.98]
$\pi(24)$	[13.50, 13.71]
$\pi(25)$	[13.29, 13.47]
$\pi(26)$	[13.08, 13.26]
...	...

Table 3. Range of occurrence of the different behavioural modes, as a function of λ_n, for $g_{K,C} = 27.24$

Burst modes	Intervals of λ_n at $g_{K,C} = 27.24$
$\pi(1)$	[220, 252]
$\pi(2)$	[253, 261]
$\pi(3)$	[268, 276]
$\pi(4)$	[279, 287]
$\pi(5)$	[288, 296]
$\pi(6)$	[297, 303]
$\pi(7)$	[304, 310]
...	...

This means that the fixed point x^* of the Poincaré map f in Fig. 5c is a snap-back repeller. Marotto (1978) showed that the existence of a snap-back repeller is sufficient for chaos.

Simply speaking, by snap-back repeller of a Poincaré map we mean that: (i) there exists a locally unstable fixed point x^* or repeller; (ii) there exists at least an orbit, starting from the vicinity of the fixed point, which is repelled far away from the vicinity and then is snapped back to the fixed point x^*. In Fig. 5c, we show an orbit starting at a point close to the fixed point x^*. In the vicinity of the fixed point x^*, the orbit is repelled because of the instability of x^*, and once it goes far away from x^* it is snapped back to x^*. This shows that the fixed point x^* is a snap-back repeller.

So, a map with a snap-back repeller implies two mechanisms: repelling the orbit that is visiting in the vicinity of the fixed point, and snapping the orbit back into the vicinity of the fixed point when far away from it. Occasionally, some orbits will be snapped back to the fixed point (the orbit shown in Fig. 5c is one example). However, most orbits will not be snapped back to the fixed point x^*, but into the vicinity of the fixed point and then be repelled far away from it. As illustrated in Fig. 5d, an orbit is repelled from the vicinity of x^* or snapped back into the vicinity randomly, but is never trapped to the fixed point x^*. In this way, the orbit exhibits irregular or chaotic behavior. This is, the snap-back repeller x^* of the map f implies chaos.

Similarly, we can also show that the map shown in Fig. 5a is chaotic.

5 Discussion

In this paper, we have shown that a simple three-variable model can lead to an enormously complex bifurcating structure, including several types of chaos as two bifurcation parameters ($g_{K,C}$ and λ_n) are varied. Some of the phenomena predicted from this model include the threshold low-amplitude oscillations before bursting, the damped burst, and the period-adding bifurcations without chaos. These predicted phenomena closely resemble those observed experimentally in various types of excitable cells under in vivo conditions (Dean and Matthews 1970; Guttman and Barnhill 1970; Huizinga et al. 1984a, b; Llinás and Yarom 1986; Takeuchi 1978).

Chaotic bursting regimes have been detected in the parameter range of $215 < \lambda_n < 240$ and $11.40 < g_{K,C} < 14.22$. In this range, the bifurcation structures evolved in the Chay model, including period-doubling and saddle-node, are similar to those described in the Rose–Hindmarsh model (Holden and Fan 1992a,b). However, there are some significant differences between the two models. First, between repetitive spikings in the Chay model complex bursting behaviors exist, such as intermittent chaotic regimes and crisis transition. Second, a bifurcation process observed in the Chay model is dominated by period-adding bifurcation. This kind of bifurcation gives rise to the generation of multispike bursting oscillation in the region of $250 \leqslant \lambda_n \leqslant 340$ and $g_{K,C} \in [10, 27.24]$. Third, the Chay model switches on action potentials in a different way from that in the Rose–Hindmarsh model. As described by Holden and Fan (1992a, b), repetitive spiking in the Rose–Hindmarsh model was formed directly from a limit cycle by gradually increasing the amplitude of the oscillation; burstings were generated via period-doubling bifurcation. In the Chay model, a threshold transition has been described as a mechanism that triggers bursting action potentials at the threshold value $G^*_{K,C}$. For the parameter $g_{K,C}$ greater than the threshold, the model exhibits either a resting potential or a low-amplitude oscillating potential, and no action potential is produced. For the $g_{K,C}$ smaller than the threshold, a complex limit cycle oscillation abruptly takes place, i.e., the Chay model triggers bursting action potentials at the threshold. This threshold transition has been termed all-or-none behavior (Plonsey 1969). Also, such threshold oscillations have been experimentally observed in neuronal cells (Llinás and Yarom 1986). Fourth, a phase transition from multispike bursting to damped bursting takes place in the range of $\lambda_n \in [340, 380]$. For $\lambda_n > 380$ and $g_{K,C} > 27.24$, the Chay model exhibits damped bursting. The damped burst wave and square wave bursting both closely simulate the

bursting action potential of muscle cells (Huizinga et al. 1984a, b; Takeuchi 1978).

These types of complex bifurcating structures exposed in the Chay model are driven by the Ca^{2+}-sensitive K^+ channel that is slowly activated by the intracellular Ca^{2+} concentration, $[Ca^{2+}]_i$. Since the formulation of the three-variable model (1), experimental evidence indicates that it may not be a Ca^{2+}-sensitive K^+ channel that is driving the bursting but rather the inactivation of Ca^{2+} channels by Ca^{2+} ions that causes the bursting (Kramer and Zucker 1985). In addition, measurements with Ca^{2+}-sensitive dye in various cells indicate that $[Ca^{2+}]_i$ changes rather fast as the membrane potential varies.

One of us has recently presented several alternative dynamic models (Chay 1987; 1990b, c, 1991) that account for the experimental evidence discussed above. In the Appendix, we present four representative models among those. In models I and II, the bursting is caused by inactivation of I_{Ca} by slowly changing $[Ca^{2+}]_i$ (Chay 1987, 1991). This model contains the same three dynamic variables as in the model analyzed here, i.e., the slowly varying $[Ca^{2+}]_i$, the fast varying n-dynamic variable, and the dependent variable V. In model II, the bursting is caused by inactivation of I_{Ca} in a voltage- and time-dependent manner (Chay 1990a). In this model, $[Ca^{2+}]_i$ is replaced by the inactivation dynamic variable f which is time- and voltage-dependent. In models III and IV, the spiking is driven by a Ca^{2+}-sensitive and V-dependent K^+ channel that is activated by the fast varying $[Ca^{2+}]_i$, and the bursting is driven by a conformational transformation of the Ca^{2+} channels (Chay 1990b, c). This transformation is induced by Ca^{2+} ions (or a Ca^{2+}-binding protein) when Ca^{2+} ion binds to the receptor site of the Ca^{2+} channels. In this model, $[Ca^{2+}]_i$ is a fast dynamic variable, and the inactivation variable f is a slow dynamic variable and is a function of voltage and time.

Our preliminary studies showed that all these models contain bifurcation structures similar to the ones presented in this paper. Since the original Chay model is sufficient to explain the observed electrical activity discussed in this paper, a more elaborate model (which includes more variables and more channels) may not be necessary in studying these types of phenomena.

To reiterate, two hypotheses exist as to why excitable cells burst: (i) a slowly activating outward K^+ current during the plateau and (ii) a slowly inactivating inward Ca^{2+} current during the plateau. The model treated here is based on the first hypothesis, while those presented in the Appendix are all based on the second hypothesis. Both hypotheses deserve some merit, since experimental evidence indicates that either one is possible (Kramer and Zucker 1985; Ammala et al. 1991). It is difficult to distinguish theoretically which of the two hypotheses is correct since activation of the slow K^+ current can have exactly the same effect as inactivation of the Ca^{2+} current. Perhaps neurons make use of both mechanisms depending on the environmental conditions. Because the two mechanisms are mathematically indistinguishable, the predictions given in this paper will apply equally well under the second hypothesis.

In the Chay model, the probability for the opening of the calcium-sensitive K^+ channel (p) is a slowly varying variable. The slowness of the probability p is modelled by a slowly changing intracellular calcium concentration, $[Ca^{2+}]_i$, i.e., $p = C/(1 + C)$. Measurements with Ca^{2+}-sensitive dyes in various cells indicate that $[Ca^{2+}]_i$ changes rather quickly with varying membrane potential (*e.g.*, Valdeolmillos et al. 1989). This contradicts the hypothesis of the model. However, it should be pointed out that the exact functional form of p is not essential for the genesis of the bursting (for illustration, see Chay 1983). The essential feature of the bursting is that p is a slow dynamic variable and has the property that it increases during depolarization and decreases during repolarization. The Chay model certainly satisfies this condition, and the results obtained in this paper can be interpreted in terms of the variable p (i.e., replace C by p).

Our bifurcation study demonstrates how easily a rhythmic neuron may be converted to a burster when two model parameters, $g_{K,C}$ and λ_n, change slightly. But what does it mean physiologically when the system bifurcates for varying values of $g_{K,C}$ and λ_n? A variation of $g_{K,C}$ mimics the effect of epileptogenic and convulsant agents; on the other hand, a variation of λ_n mimics a change in temperature. In fact, it has been demonstrated (Chalazonitis 1978) that the application of epileptogenic agents to the soma of rhythmic *Helix* cells leads to an appearance of square-wave bursting and a relaxation oscillation (which resemble those simulated in this paper). Elimination of the drug by washing converts back to repetitive rhythmic activity. Thus, a variation of $g_{K,C}$ implies abnormal electrical activity that results in epilepsy. An abnormal environmental condition, such as hyperthermia, may also convert regular rhythmic to paroxysmal activity. Bursting activity induced by a rise in temperature may explain the well-known febrile convulsions of children.

Chaos similar to that simulated in this paper has been discovered in many neuronal cells (see, for example, Chalazonitis and Boisson 1978). Presently, the resolution of a digitizer that records a neuronal voltage signal is not accurate enough to distinguish whether the chaos found in this recording is due to stochastic or deterministic chaos. However, our demonstration that various types of chaos arise in a simple neuronal model system suggests that the disordered behavior observed in these neuronal systems must be governed by deterministic rules. To demonstrate the deterministic nature of chaotic recordings, one may construct one-dimensional maps that relate the previous spike interval I_{i-1} to the present one I_i (Chay 1986). With three maps, one can see whether these recordings follow the deterministic rules found in this paper. Also, their route to chaos can be investigated by varying the bifurcation parameters (e.g., drug concentration or temperature). With an advent of improved recording techniques and isolated experimental preparations, it will soon be possible to perform such experiments where the bifurcation parameters can be precisely controlled (Rapp 1993). Our mathematical predictions presented in this paper can then be used to guard against fallacious conclusions.

We believe that the elucidation of abnormal electrogenesis in terms of the ionic mechanism presented in this paper will lead to a greater understanding of the intrinsic, nonlinear, dynamic properties of neurons after chemical or temperature modifications.

Appendix. Three-variable models based on Ca^{2+} channel inactivation

A.1 Model I

The model was presented in Chay (1987).

$$-dV/dt = g_c d_\infty f_\infty (V - V_C) + g_K n(V - V_K) + g_L(V - V_L)$$

$$dn/dt = (n_\infty - n)/\tau_n$$

$$dC/dt = [d_\infty f_\infty (V_C - V) - k_C C]/\tau_C$$

where

$$d_\infty = 1/\{1 + \exp[(V_d - V)/S_d]\} \text{ and}$$

$$f_\infty = 1/\{1 + \exp[(V_f - V)/S_f]\}$$

$$V_f = S_f n_H \ln(C/K_f)$$

$$n_\infty = 1/\{1 + \exp[(V_n - V)/S_n]\} \text{ and}$$

$$\tau_n = \tau_n^*/\{1 + \exp[(V - V_n)/S_n]\}$$

The parametric values are: $g_C = 55$, $g_K = 280$, $g_L = 2.2$, $V_C = 100$, $V_K = -80$, $V_L = -40$, $V_d = -22$, $S_d = 7.5$, $V_n = -9$, $S_n = 10$, $S_h = 10$, $\tau_C = 4000$, and $\tau_n^* = 0.0085$, $K_f = 1$, $k_C = 75$, $n_H = 3$. The two bifurcation parameters that give rise to the interesting bursting and chaotic behaviors are V_f and τ_n^*.

A.2 Model II

The model was presented in Chay (1991).

$$-dV/dt = \Sigma I_{ionic} = I_f + I_s + I_K + I_L$$

$$dn/dt = (n_\infty - n)/\tau_n$$

$$dC/dt = [d_\infty f_C (V_s - V) - k_C C]/\tau_C$$

where

$$I_f = g_f m_\infty (V - V_f),$$

$$I_s = g_s d_\infty f_C (V - V_s)$$

$$I_K = g_K n(V - V_K);$$

$$I_L = g_L(V - V_L).$$

and

$$y_\infty = 1/\{1 + \exp[(V_y - V)/S_y]\}, \; y \text{ stands for } d, f, \text{ and } n;$$

$$f_C = 1/(1 + C)$$

$$\tau_n = \tau_n^*/\{1 + \exp[(V - V_n)/S_n]\}$$

The parametric values of model I are: $g_f = 60$, $g_s = 25$, $g_K = 110$, $g_L = 25$, $V_f = 40$, $V_s = 110$, $V_K = -80$, $V_L = -60$, $V_m = -18$, $S_m = 8$, $V_d = -40$, $S_d = 8$, $V_n = -10$, $S_n = 8$, $\tau_C = 40$, $\tau_n^* = 0.026$, and $k_C = 2$. The two bifurcation parameters that give rise to the interesting bursting and chaotic behaviors are k_C and τ_n^*.

A.3 Model III

The model was presented in Chay (1990a).

$$-dV/dt = \Sigma I_{ionic} = I_s + I_K + I_L$$

$$df/dt = (f_\infty - f)/\tau_f$$

$$dn/dt = (n_\infty - n)/\tau_n$$

where

$$I_s = g_s d_\infty f(V - V_s)$$

$$I_K = g_K n(V - V_K)$$

$$I_L = g_L(V - V_L).$$

and

$$y_\infty = 1/\{1 + \exp[(V_y - V)/S_y]\}, \; y \text{ stands for } d, f, \text{ and } n$$

$$\tau_f = \tau_f^*/\{\exp(V_f - V)/2S_f + \exp(V - V_f)/2S_f\}$$

$$\tau_n = \tau_n^*/\{1 + \exp[(V - V_n)/S_n]\}$$

The parametric values of model III are: $g_s = 200$, $g_K = 250$, $g_L = 13$, $V_s = 40$, $V_K = -80$, $V_L = -60$, $V_d = -18$, $S_d = 8$, $V_f = -40$, $S_f = -10$, $V_n = -5$, $S_n = 10$, $\tau_f^* = 40$ and $\tau_n^* = 0.012$. The two bifurcation parameters that give rise to the interesting bursting and chaos behaviors are V_f and τ_n^*.

A.4 Model IV

This model was presented in Chay (1990b).

$$-dV/dt = \Sigma I_{ionic} = I_s + I_{K,C} + I_L$$

$$df/dt = (f_\infty - f)/\tau_f$$

$$dC/dt = [d_\infty f h_C (V_s - V) - k_C C]/\tau_C$$

where

$$I_s = g_s d_\infty f h_C (V - V_s)$$

$$I_{K,Ca} = g_{K,C} n_\infty (V - V_K)$$

$$I_L = g_L(V - V_L)$$

and

$$y_\infty = 1/\{1 + \exp[(V_y - V)/S_y]\}, \; y \text{ stands for } d, f, \text{ and } n$$

$$\tau_f = \tau_f^*/\{\exp(V_f - V)/2S_f + \exp(V - V_f)/2S_f\}$$

$$h_C = 1/(1 + C)$$

$$V_n = -35 \ln(C/K_n)$$

The parametric values of model IV are: $g_s = 400$, $g_{K,C} = 9000$, $g_L = 25$, $V_s = 100$, $V_K = -90$, $V_L = -60$, $V_d = -13$, $S_d = 8$, $V_f = -40$, $S_f = -10$, $S_n = 13$, $\tau_f^* = 40$, $\tau_C = 0.06$, $k_C = 2$, and $k_n = 10$. Note here that (unlike models I and II) V_n is not constant but is a function of C. The two bifurcation parameters that give rise to the interesting bursting and chaos behaviors are V_f and τ_C.

Acknowledgements. This work was supported by a grant from the Pennsylvania Affiliate of the American Heart Association Foundation and by NSF DCB-8919245. This research was also supported in part by a grant from Pittsburgh Supercomputer Center through the NIH division of Research Resources Cooperative Agreement U41 RR0415.

References

Ammala C et al. (1991) Inositol trisphosphate-dependent periodic activation of a Ca^{2+}-activated K^+ conductance in glucose-stimulated pancreatic β-cells. Nature 353:849–852

Canavier CC, Clark JW, Byrne JH (1990) Routes to chaos in a model of a bursting neuron. Biophys J. 57:1245–1251

Canavier CC, Clark JW, Byrne JH (1991) Simulation of the bursting activity of neuron, R15 in *Aplysia*: role of ionic currents, calcium balance, and modulatory transmitters. J. Neurophysiol 66:2107–2124

Chalazonitis N (1978) Some intrinsic and synaptic properties of abnormal oscillators. In: Chalazonitis N, Boisson M, (eds) Abnormal neuronal discharges. Raven, New York, pp 115–132

Chalazonitis N, Boisson M (eds) (1978) Abnormal neuronal discharges. Raven, New York

Chay TR (1983) Eyring rate theory in excitable membranes: application to neuronal oscillations. J. Phys Chem 87:2935–2940

Chay TR (1984) Abnormal discharges and chaos in a neuronal model system. Biol Cybern 52:301–311

Chay TR (1985) Chaos in a three-variable model of an excitable cell. Physica 16D:233–242

Chay TR (1986) Oscillations and chaos in the pancreatic β-cell. In: Othmer H (ed) Lecture in biomathematics. Springer Berlin Heidelberg New York, pp 2–18

Chay TR (1987) The effect of inactivation of calcium channels by intracellular Ca^{2+} ions in the bursting pancreatic β-cells. Cell Biophys 11:77–90

Chay TR (1990a) Bursting excitable cell models by a slow Ca^{2+} current. J. Theor Biol 142:305–315

Chay TR (1990b) Effect of compartmentalized Ca^{2+} ions on electrical bursting activity of pancreatic β-cells. Am. J. Physiol 258 (Cell Physiol 27): C955–C965

Chay TR (1990c) Electrical bursting and intracellular Ca^{2+} oscillations in excitable cell models. Biol Cybern 63:15–23

Chay TR (1991) Complex oscillations and chaos in a simple neuron model. In: International Joint Conference on Neural Networks, Seattle, WA, July 8–12

Chay TR, Cook DL (1988) Endogenous bursting pattern in excitable cells. Math Biosci 90:139–153

Chay TR, Fan YS (1993) Evolution of periodic states and chaos in two types of neuronal models. In: Ditto WL, Chaos in biology and medicine. Proc SPIE 2036:100–114

Chay TR, Kang HS (1987) Multiple oscillatory states and chaos in the endogenous activity of excitable cells: pancreatic β-cell as an example. In: Degen H, Holden AV, Olsen LF (eds) Chaos in biological systems. Plenum, New York, pp 183–190.

Chay TR, Keizer J (1983) Minimal model for membrane oscillations in the pancreatic β-cell. Biophys J. 42:181–190

Chay TR, Lee YS (1990) Bursting, beating, and chaos by two functionally distinct inward current inactivations in excitable cells. In: Jalife J, (ed) Mathematical approaches to cardiac arrhythmias. New York Academy of Sciences 591:328–350

Dean PM, Matthews EK, (1970) Electrical activity in pancreatic islet cells: effect of ions. J. Physiol 210:265–275

Decroly O, Goldbeter A (1987) From simple to complex oscillatory behavior: analysis of bursting in a multiply regulated biochemical system. J. Theor Biol 124:219–250

Epsein IR, Marder E (1990) Multiple modes of a conditional neural oscillator. Biol Cybern 46:23–34

Fan YS, Chay TR (1993) Crisis transitions in excitable cell models. Chaos Solitons Fractals 3:603–615

Fan YS, Holden AV (1993) Bifurcations, burstings, chaos and crises in the Rose–Hindmarsh model for neuronal activity. Chaos Solitons Fractals 3:439–449

Grebogi C, Ott E, Yorke JA (1987) Critical exponents for crisis-induced intermittency. Phys Rev A36:5365

Guckenheimer J, Holmes P (1983) Nonlinear oscillations, dynamical systems and bifurcations of vector fields. (Appl Math Sci 42) Springer, Berlin Heidelberg, New York

Guevara MR, Glass L, Shrier A (1981) Phase locking, period-doubling bifurcations, and irregular dynamics in periodically stimulated cardiac cells. Science 214:1350–1355

Guttman R, Barnhill R (1970) Oscillation and repetitive firing in squid axons. J. Gen Physiol 55:104–118

Hao BL (1983) Bifurcations, chaos, strange attractor, turbulence and all that – on intrinsic stochasticity in deterministic systems. Prog Phys 3:329–416

Hayashi H, Ishizuka S (1987) Chaos in molluscan neuron. In: Degn H, Holden AV, Olsen LF (eds) Chaos in biological systems. Plenum, New York, 156–166

Hindmarsh JL, Rose RM (1982) A model of the nerve impulse using two first-order differential equations. Nature 296:162–164

Hindmarsh JL, Rose RM (1984) A model of neuronal bursting using three coupled first order differential equations. Proc R. Soc Loud Biol 221:87–102

Hodgkin AL, Huxley AF (1952) A quantitative description of membrane current and its application to conduction and excitation in nerve. J. Physiol 117:500–544

Holden AV, Fan YS (1992a) From simple to simple bursting oscillatory behavior via chaos in the Rose–Hindmarsh model for neuronal activity. Chaos Solitons Fractals 2:221–236

Holden AV, Fan YS (1992b) From simple to complex oscillatory behavior via intermittent chaos in the Rose-Hindmarsh model for neuronal activity. Chaos Solitons Fractals 2:349–369

Holden AV, Fan YS (1992c) Crisis-induced chaos in the Rose–Hindmarsh model for neuronal activity. Chaos Solitons Fractals 2:583–595

Huizinga JD, Chang G, Diamant NE, El-sharkawy TY (1984a) The effects of cholecystokinin-octapeptide and pentagastrin on electrical and motor activities of canine colonic circular muscle. Can. J. Physiol Pharmacol 62:1440–1447

Huizinga JD, Chang G, Diamant NE, El-sharkawy TY (1984b) Electrophysiological basis of excitation of canine colonic circular muscle by cholinergic agents and substance P^1, J. Pharmacol Exp Ther 231:592–599

Kaas–Petersen C, (1987) Bifurcations in the Rose–Hindmarsh and Chay models. In: Degen H, Holden AV, Olsen LF (eds) Chaos in biological systems. Plenum, New York, pp183–190

Kramer RH, Zucker RS (1985) Calcium-induced inactivation of calcium current causes the inter-burst hyperpolarization of Aplysia bursting pace-maker neurones. J. Physiol 362:131–160

Lee YS, Chay TR, Ree T (1983) On the mechanism of spiking and bursting in excitable cells. J. Biophys Chem 18:25–34

Llinás R, Yarom Y (1986) Oscillatory properties of guinea-pig inferior olivary neurones and their pharmacological modulation: an in vitro study. J. Physiol 376:163–182

Marotto H (1978) Snap-back repellers imply chaos in R^n. J. Math Anal Appl 63:199–223

Matsumoto G, Takahashi N, Hanyu Y (1987) Chaos, phase locking and normal squid axons. In: Degn H, Holden AV, Olsen LF (eds) Chaos in biological systems. Plenum, New York. pp 143–156

May R (1976) Simply mathematical models with very complicated dynamics. Nature 261:459–467

Plant RE (1981) Bifurcation and resonance on a model for bursting nerve cells. J. Math Biol 11:15

Plonsey R (1969) Bioelectric phenomena. McGraw-Hill, New York

Poincaré H, (1899) Les méthods nouvelles de la mécanique céleste. Gauthier-Villars, Paris

Rapp PE (1993) Chaos in the neurosciences: cautionary tales from the frontier, Biologist 40:89–94

Rinzel J, Lee YS (1987) Dissection of a model for neuronal parabolic bursting. J. Math Biol 25:653–657

Takeuchi H, (1978) Modifications of the convulsant-induced abnormal biopotentials of a molluscan giant neuron by drugs, divalent ions, and temperature change. In: Chalazonitis N, Boisson M, (eds) Abnormal neuronal discharge. Raven, New York

Valdeolmillos M et al. (1989) Glucose-induced oscillations of intracellular Ca^{2+} concentration resembling bursting electrical activity in single mouse islets of Langerhans. FEBS Lett 259:19–23